RSC Advances

ROYAL SOCIETY OF CHEMISTRY

www.rsc.org/advances

RSC Advances ARTICLE
www.rsc.org/advances

Highly Efficient NIR-NIR Upconversion in Potassium Substituted $CaMoO_4:Tm^{3+},Yb^{3+}$ Phosphor for Potential Biomedical Applications

Hom Nath Luitel[1,2*], Rumi Chand[1], Toshio Torikai[1], Mitsunori Yada[1], Takanori Watari[1#]

Received () Xth XXXXXXXXX 20XX, Accepted Xth XXXXXXXXX 20XX
DOI:

Highly efficient NIR to NIR (excitation by 980 nm, emission at 800 nm) upconversion in $CaMoO_4:Tm^{3+},Yb^{3+},M^+$ (M=Li, Na, K, Rb) nanocrystals were synthesized by a hydrothermal method. The XRD patterns show that they are all tetragonal structure despite of small amount of RE^{3+} and M^+ ions doping. The solid solubility of lithium, sodium, potassium and rubidium ions in the $CaMoO_4$ were found to be 30 mol%, 20 mol%, 10 mol% and 5 mol%, respectively. The doped M^+ ions affect the crystal field symmetry around Tm^{3+} ions in the $CaMoO_4$ host, which results in the change of the irradiation transition probabilities between their transition levels and intensify the UC intensities. Compared with $CaMoO_4:Tm^{3+},Yb^{3+}$, the NIR to NIR upconversion emission intensity of $CaMoO_4:Tm^{3+},Yb^{3+},0.10M^+$ nanocrystals increases by 2.2, 3.3, 47, 10 folds for Li, Na, K and Rb, respectively. The K substituted $CaMoO_4:Tm^{3+},Yb^{3+}$ phosphor exhibited intense UC emission pumped by less than 1 mW laser power and can have potential application in NIR to NIR photodynamic diagnosis.

1. Introduction

Photon upconversion involves the absorption of several photons of low energy with subsequent emission of higher energy photons. Various processes can lead to upconversion, including two/three-photon absorptions, ground state followed by excited state absorption, energy transfer upconversion, second harmonic generation, and photon avalanche.[1,2] Since its discovery in the 1960s, upconversion (UC) has been the focus of many researchers.[3-11] These UC materials with strong luminescence in the NIR to visible or NUV region has been extensively investigated in recent years due to their several potential applications in solar cells,[4] novel display technologies,[5] inks for secure printing,[6,7] optical communication and amplifier,[8] high density optical storage,[9] infrared detection and sensors,[10] and more recently bio medical diagnosis and therapies.[11]

Currently organic dyes and fluorescence proteins are being used for bioimaging.[12,13] However, they suffer severely due to low sensitivity, a short lifetime, very small stokes shift in aqueous solution, photobleaching during exposure to light and limited observation depth due to very low penetration depth of UV in the body tissue.[14] Absorption and scattering of the photons induced by biological tissue and water molecules are the major factors that lead to attenuation of signal proportional to the depth of the feature of the interest, especially in the visible imaging range (400 nm ~ 750 nm).[15] To overcome these problems, imaging agents with improved photo-physical properties in the biological transparency window (650 nm ~ 1450 nm) are essential, where the biological tissue scatter and absorb less light at longer wavelengths, resulting in deeper penetration than the traditional visible light.[16] Upconverting nano materials could indeed be used as probes for single molecule imaging in biological cells.[17,18] These UCNPs excited by NIR light source overcome these limitations because these UCNPs are chemically stable with no photobleaching effect, wide stokes shift and good penetration depth of source light because the used NIR source can penetrate deep into the body tissue. However, present UCNPs suffer badly due to their low efficiency.[19,20] In UC based techniques, detection sensitivity depends on the luminescence intensity of the phosphor. Recently, several attempts have been made to increase the luminescence intensity of upconversion nanoparticles (UCNP), such as co-doping with sensitizer ions,[2,21,22] crystal surface coating,[22,23] core/shell synthesis,[24] *etc.*, but most of them are not enough to improve the UC intensity to desire level (should be pumped by as low as 1 mW laser power to protect the body tissue being overheated). Hence, the luminescence intensity enhancement of UCNPs is still a challenging topic. Mainly, the UC intensity is governed by following three factors: (1) high electronic transition probabilities of the dopants,[25,26] (2) The energy transfer rate from sensitizer (Yb^{3+}) to emission center (Tm^{3+}, Er^{3+}, Ho^{3+} *etc.*) depends on the overlap of the transition dipoles of these two ions. Thus, the distances between Yb^{3+} and Tm^{3+} (Er^{3+}, Ho^{3+} *etc.*) ions affect the energy transfer and migration and the UC intensity,[22] and (3) The local environment of RE^{3+} ions in the host lattice. The crystal field, which is responsible for breaking the selection rule for the forbidden 4f–4f transitions of RE^{3+} ions, originates from the atoms surrounding the RE^{3+} ions.[27]

To date, hexagonal $NaYF_4$ is the most researched and efficient host material for green, red and blue UC in which NIR excitation is absorbed by the Yb^{3+} ion and UC luminescence emitted by Er^{3+} or Tm^{3+}, respectively.[22,28] More recently, much attention has been focused on tuning the UC spectra. For instance, Huang *et al.* reported that small amount of Sc^{3+} ions doping results the higher UC intensity.[29] The Sc^{3+} ions occupies the Y^{3+} position in $NaYF_4$ lattice. Since the Sc^{3+} ion is smaller than Y^{3+} ion, small amount of Sc^{3+} doping will destroy the local symmetry around the emission center resulting in the higher UC intensity. Teng *et al.* synthesized Na_xScF_{3+x}:Yb,Er nanocrystals and studied the effect of polarity of the reaction medium on the phase and composition of the nanocrystals and used Sc^{3+} doped crystals for multicolor tuning.[30] Dou *et al.* tuned the UC spectra by doping different alkali metal ions in to $NaYF_4$:Yb,Er.[31] They reported no UC emission intensity enhancement, but the blue/green, blue/red, and green/red emission intensity ratios were affected by the concentration of Li^+ and K^+.[28] Sing *et al.* explored the PL emission enhancement of the phosphor by Li^+ doping.[32] Compared to the huge number of studies on the $NaYF_4$:Yb,Er nanocrystals, very small effort has been paid on the work of oxide based UC phosphors.[33,34] Moreover, the study of NIR to NIR UC luminescence has not been in focus despite most suitable spectral range for the bioimaging due to best match of optical window of body tissue (750-1450 nm) with NIR to NIR UC.[35]

Herein, we report controlled synthesis of $CaMoO_4:Tm^{3+}$, Yb^{3+} phosphor with various alkali metal ions substitution via simple hydrothermal method and their effect on the NIR to NIR UC luminescence properties.

2. Experimental

2.1 Sample preparation

Calcium molybdate phosphors doped with Tm^{3+} and Yb^{3+} ions, $CaMoO_4:Tm^{3+},Yb^{3+}$, were prepared by hydrothermal (HT) process. In a typical hydrothermal reaction, 10 mM mixture of Ca/Yb/Tm ($Ca(NO_3)_2.4H_2O$/$Yb(NO_3)_3.5H_2O$/$Tm(NO_3).5H_2O$) were prepared in

a beaker with distilled water by constant stirring with magnetic stirrer. In a separate beaker, 10 mM $(NH_4)_6Mo_7O_{24}\cdot 4H_2O$ was prepared in distilled water. 10 mM Citric acid or PEG-2000 or Cetyltrimethylammonium bromide (CTAB) were used as structure directing agent (the ratio of metal ions to structure directing agents being 1 to 1) and urea as precipitating agent (if necessary). The pH of the resulting solution was adjusted by aqueous ammonia solution. The pH of solution containing CTAB, PEG and Citric acid were adjusted to ~9, ~5 and ~2, respectively. Then, 30 ml of the mixture was poured into a 50 ml Teflon lined stainless steel autoclave and kept at 180~200 ℃ for various time periods. In case of alkali metal ions substituted samples, appropriate amount of MNO_3 (M = Li, Na, K, Rb) were added into the Ca solution before mixed with the Mo solution. The solid obtained was centrifuged, washed multiple times with distilled water followed by ethanol and freeze dried for 12 hours. The powder sample was further calcined at various temperatures from 500 ℃ to 800 ℃ for 1 h to get the final highly crystalline oxide phosphor product. For comparison, samples of $CaMoO_4$:Tm^{3+},Yb^{3+} were also prepared by solid state reaction method. In the solid state reaction, analytic grade $CaCO_3$, MoO_3, Yb_2O_3, Tm_2O_3 and M_2CO_3 (M = Li, Na, K, Rb) were mixed thoroughly with the help of ethanol in mortar and pestle, dried in air and calcined at 650 ºC for 3h.

2.2 Characterizations

Phase identification was carried out using a Shimadzu XRD-6300 instrument with Cu Kα radiation. The lattice constants were evaluated using cellcalc ver. 2.20. The hkl and d values obtained from the XRD measurements were used for the lattice constant calculations. The morphology of the phosphor particles were characterized by scanning electron microscopy (Hitachi-S3000N). Elemental analysis and mass percentage of the constituent ions were estimated using EDX coupled with SEM. Before SEM measurements, each sample was coated roughly 5 nm in thickness with platinum-palladium using Hitachi E-1030 ion sputter. Fourier transform infrared spectroscopy (FT-IR) data were collected on a Hitachi 4000 FT-IR spectrophotometer in the range of 400–4000 cm^{-1} using KBr powder. Elemental composition of the final phosphor products were analysed using X-ray fluorescence spectrometer (Shimadsu, Rayny-107 series). UC emission spectra, pumped by a 980 nm cw laser (0-200 mW), were recorded using USB 4000 UV-VIS-NIR miniature fiber optic spectrometer (Ocean optics). All measurements were carried out at room temperature unless specified.

3. Results and discussion

Figure 1 presents the phase analysis of $CaMoO_4$ doped with 0.1 mol% Tm^{3+}, 10 mol% Yb^{3+} and 0~30 mol% K^+. The XRD patterns in Fig. 1(a) agree well with standard pattern of JCPDS (29-0351) and no secondary phases could be identified with variation of K^+ concentrations at low level (up to 10 mol%). The $CaMoO_4$ consists of tetragonal structure with I41/a space group. The lattice constants of the 0 mol% K substituted sample calculated from the XRD data are; a = b = 5.20 Å and c = 11.445 Å, similar to the reported data [JCPDS: 29-0351]. However, with the increase of the K^+ concentrations above 10 mol%, secondary phases $KYb(MO_4)_2$ (JCPDS: 52-1688) and $K_2Mo_2O_7$ (JCPDS: 36-0347) appeared indicating that the solid solubility limit of K^+ in the $CaMoO_4$ phase is 10 mol%. A similar study was carried out by substituting part of Ca by other alkali metal ions *viz.* Li^+, Na^+ and Rb^+ and the results are presented in supplementary Fig. S1. Up to 10 mol% M^+ ions substitution, no secondary phases were observed for three alkali metal ions, except Rb^+. The solid solubility limit for various alkali metal ions obtained were 30 mol%, 20 mol%, 10 mol% and about 5 mol% for Li^+, Na^+, K^+ and Rb^+, respectively. Fig. 1(b) summarises the lattice parameters of $CaMoO_4$ with various moles of K^+ substitution. It is clear that with the substitution of K^+, the cell volume gradually increased up to 10 mol% K^+, and above that it gradually decreased, which confirms that the substitution of Ca by bigger potassium increased the cell volume. The slight decrease of cell parameters above 10 mol% might be due to secondary phase which significantly alters the cell parameters under consideration.

The purity of the $CaMoO_4$ phase was further confirmed by FT-IR analysis as shown in Fig. S2. The broad bands around 3450 cm^{-1} and 1618 cm^{-1} were assigned to the O-H stretching and H-O-H bending vibrations of the water molecules which are prominent in the $(NH_4)_6Mo_7O_{24}\cdot 4H_2O$ molecules.[36] Water molecules get absorbed by $CaMoO_4$ phosphor and relatively weak peaks corresponding to water molecules were observed in case of HT product as well. Very strong absorption bands around 700 ~ 970 cm^{-1} are related to the O-Mo-O stretches of the MoO_4 tetrahedron.[37] The absorption bands centered around 940 cm^{-1}, 770 cm^{-1} and 430 cm^{-1} (not shown here) are the v_1, v_3 and v_2 modes of the MoO_4 groups which suggests that the product was pure $CaMoO_4$ and did not contained polymeric molybdenum compounds.[38]

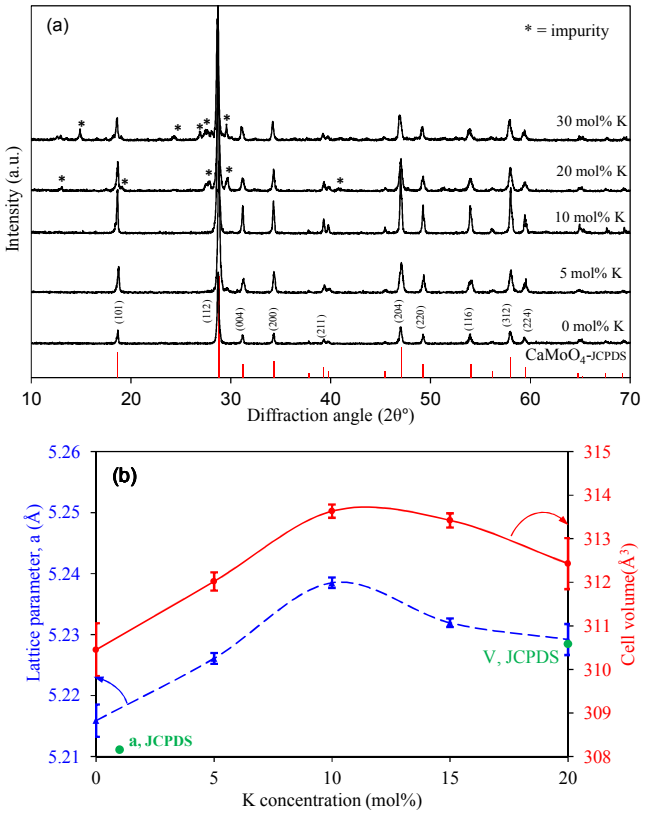

Fig. 1. XRD patterns of various moles of K^+ substituted $CaMoO_4$:0.001Tm^{3+},0.1Yb^{3+} phosphors (a) and varioation of lattice parameters with K substitution (b).

The particles morphology, size distribution and elemental composition were insvestigated using SEM (EDX), as shown in Fig. 2. Fine particles with rice grains shape, agglomerated thin plates and spherical balls were obtained during the hydrothermal treatment whereas finely sintered compact ceramics was observed during solid state reactions. Fig. 2(a) shows that agglomeration free nanoparticles of rice grains with diameter of about 100 nm and length of about few hundreds of nanometers were obtained when the HT was carried out in the presence of CTAB at relatively higher pH of ~9. Fig. 2(b) shows that thin flakes agglomerated with each other forming bigger structures when PEG-2000 was used as surfactants at pH 4 ~ 7. Whereas, spherical balls composed of numerous nanograins were obtained while citric acid/urea assisted HT treatment was carried out at relatively lower pH 1 ~ 2. Obviously, the solid state sample exhibits dense compacts consisting of spherical to irregular particulates of 1 to 3 μm.

The growth mechanism of the various particles shapes and sizes during hydrothermal treatment assisted by growth directing agents have been previously reported by many authors[39,40,41] and can be explained as in supporting Fig. S3. First, calcium ions get complexes with surfactants and forms calcium-surfactant complex. Ion exchange with molybdenum ions followed by precipitation forms calcium molybdates. These calcium molybdates or its hydrates forms crystal nucleus or nanograins. Unidirectional growth of calcium molybdates nanograins forms different shapes during the hydrothermal treatment process due to the presence of growth directing agent, here citric acid or PEG-2000 or CTAB. In case of rice grains, during the hydrothermal treatment these nanograins get self-assembled along c-axis and forms elongated particles which grows with hydrothermal treatment time to generate rice grains. The rice grains size is expected to increase with the HT process time as shown in the TEM images of the supporting Fig. S4. In the case of balls formation, the nanograins arrange themselves radially from the core, presumable because of the presence of excess citric acid molecule. Numerous nanograins self-assemble into a ball like structure getting bigger and bigger structures. Then during the hydrothermal treatment these self-assembled balls rolled over forming smooth, dense and ordered structures. If the growth direction is two dimentional along the a and b axis, plates-like structures is expected. Here, long chain molecules of PEG protect the growth of the calcium molybdate along the c-axis resulting thin plates. Further, larger the concentration of the PEG molecules, thinner plates will be expected.

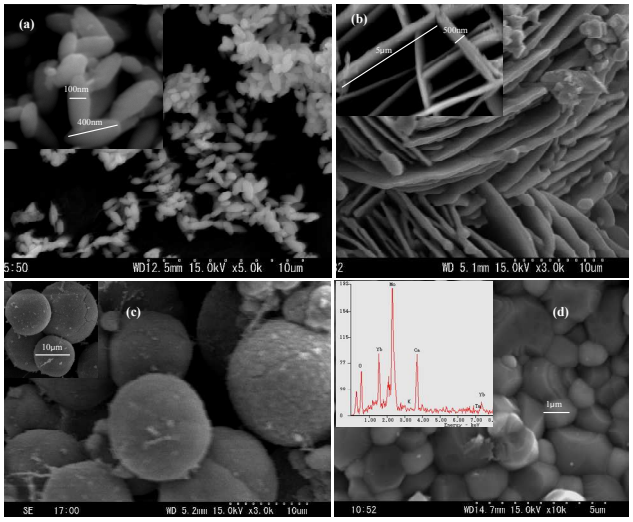

Fig. **2**. SEM images of $CaMoO_4$:0.1 mol% Tm, 10 mol% Yb phosphors hydrothermally treated at pH 9 using CTAB (a), pH ~5 using PEG-2000 (b), pH ~ 2 using citic acid/urea (c), and solid state sample (d) with typical EDS spectrum (inset of d).

Following 980 nm laser excitation at room temperature, $CaMoO_4$:0.001Tm^{3+},0.1Yb^{3+} phosphor exhibits intense NIR emission (~797 nm) and a weak blue emission (477 nm). Typical emission spectra (Fig. 3) show an intense emission corresponding to the intra 4f-4f $^3H_4 \rightarrow {}^3H_6$ electronic trasition of Tm^{3+} ion around 797 nm (NIR), and a very weak blue emission assigned to the $^1G_4 \rightarrow {}^3H_6$ electronic trasition around 477 nm.[28,35] We have carefully monitered the Tm^{3+} ions concentration (as shown in Fig. 3) and found that the optimum concentration for the better NIR and blue emissions is ~0.1 mol%. Above 0.1 mol% Tm^{3+} concentration, gradual quenching of the emission occurred due to concentration quenching process where the excited electrons relaxed non radiatively.[43] The NIR emission band is almost 10 fold stronger than the blue emission band and our target is NIR emission at ~800 nm, hereafter we discuss the improvements of the NIR emission only.

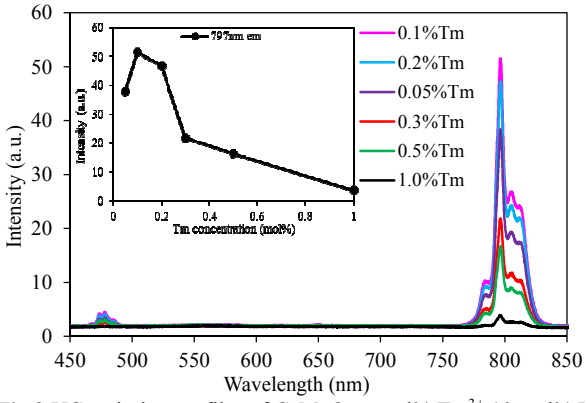

Fig.3 UC emission profiles of $CaMoO_4$:x mol% Tm^{3+},10 mol% Yb^{3+} phosphors. Inset shows the variation of UC emission intensity at 477 nm and 797 nm according to Tm content.

Fig. 4 represents the effect of Yb^{3+} ions concentration at fixed Tm^{3+} ions concentration (0.1 mol%). As shown in the inset in Fig. 4, at fixed Tm^{3+} ions concentration, the intensities of the NIR emission at 797 nm gradually increased with Yb^{3+} ions concentration up to 10 mol% and then decreased at concentrations over 10 mol% due to concentration quenching process.[43] This concentration quenching effect could be explained by the energy transfer between the nearest dopants (either activator to activators or activators to sensitizers or sensitizer to sensitizer). As the dopants concentration increased, the distance between dopants ions shrinks allowing non-radiative energy migration such as exchange, dipole or multi-pole interactions. As summarized in the insets of Fig. 4, the optimum Yb^{3+} concentrations was 10 mol%. Further, at higher rare earth ions concentrations, the solid solubility limits reached the maximum and a secondary phase appears which hampers the UC emission.[2,42]

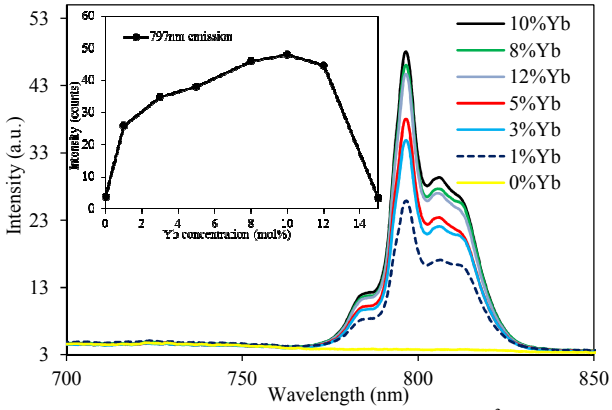

Fig. 4. UC emission profiles of $CaMoO_4$:0.1 mol% Tm^{3+}, y mol% Yb^{3+} phosphors. Inset shows the variation of UC emission intensity at 797 nm according to Yb content.

It is speculated that the addition of Tm^{3+} and Yb^{3+} ions in to the Ca^{2+} sites in $CaMoO_4$ lattice produces stress due to charge imbalance. Thus, charge neutrality demands removal of three Ca^{2+} sites to introduce two Tm^{3+} or Yb^{3+} ions, which eventually restricts the Tm^{3+}/Yb^{3+} ions solubility. Due to restricted solubility of rare earth ions in the host lattice, several efforts has been made recently to increase the emission efficiency of the rare earth ions doped phosphors.[42,44,45,46] Use of monovalent charge compensator ions (such as Li^+, Na^+, K^+, Ag^+ *etc*) showed promising effect on the enhancement of emission intensity of the alkali or alkaline earth based materials.[42,47,48] S. Das *et al.* explained that the K^+ ions substitution on the $CaSO_4$:Dy^{3+} enhance the PL intensity significantly.[47] J.H. Chung *et al.* significantly increased the UC intensity of $CaMoO_4$ blue phosphor by excess Li^+ ions addition.[44]

Further, substitution of part of divalent Ca^{2+} ions (0.114Å) by monovalent K^+ ion (0.152 Å) is expected to distort the crystal field of Tm^{3+} ions in the $CaMoO_4$ significantly due to size and charge difference. Herein, we have systematically investigated the effect of various alkali metal ions (Li^+, Na^+, K^+ and Rb^+) on the phase stability of Tm^{3+}/Yb^{3+} doped $CaMoO_4$ and its UC luminescence.

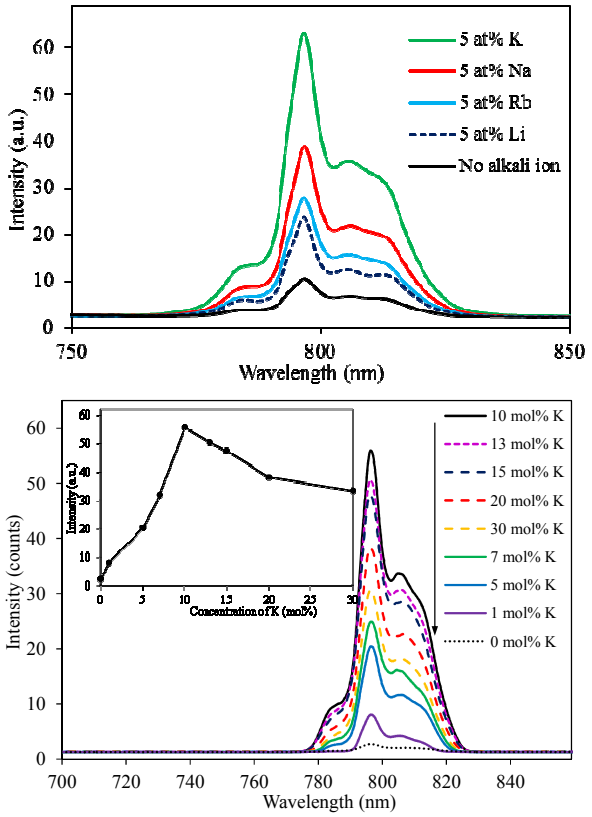

Fig. 5. UC emission profiles of $CaMoO_4$:0.1 mol% Tm^{3+}, 10 mol% Yb^{3+}, 5 mol% M^+ phosphors (a) and effect of K^+ ions concentrations on UC intensities (b).

Fig. 5(a) shows the effect of 5 mol% M^+ ions (Li^+, Na^+, K^+ and Rb^+) substitution on the $CaMoO_4$:0.1 mol% Tm, 10 mol% Yb phosphor. Obviously, substitution of alkali metal ions significantly intensified the UC emission at NIR band and the order of increment is as; K^+>Na^+>Rb^+>Li^+>no alkali ion. Substitution of 5 mol% K intensified the UC emission by almost 6 fold to that of without alkali ions. Since, K^+ substitution exhibited better UC intensity, effect of K^+ ions concentration was studied within small increment and the result is presented in Fig. 5(b). It is clear that K^+ ions substitution gradually increased the UC emission intensity up to 10 mol% and above 10 mol% again decreased indicating the limit of K substitution. As seen from the XRD in Fig.1, the doping ($Tm^{3+}/Yb^{3+}/K^+$ ions) showed no significant change in the crystal structure (no new phase was generated), suggesting these doped ions have occupied the cataionic sites in the host lattice structures. Further we have confirmed the amount of K^+ ions present in the $CaMoO_4$ host after calcination at 650℃ for 1 h by X-ray fluorescence spectroscopy and the results are presented in table 1. It is clear that the amount of K^+ ions used in the reaction mixture incorporated in to the $CaMoO_4$ host. It is believed that K^+ ions forms solid solution with the $CaMoO_4$ host and gets precipitated during the reaction. As shown in Fig. 5(b), a monotonic increase in UC intensities up to 47 folds with K^+ concentrations (up to 10 mol%) was observed. However, at higher K^+ concentrations, new phases $K_2Mo_2O_7$ (JCPDS: 36-0347) and $KYb(MO_4)_2$ (JCPDS: 52-1688) appeared which are non emissive and reduced the UC intensity. Two factors plays important roles for the improvements of UC intensities by K^+ susbtitution, one the K^+ doping facilitates the solubilization of rare earth ions into the $CaMoO_4$ matrix by allowing the Tm^{3+}/Yb^{3+} ions to accupy the Ca^{2+} sites through charge balance mechanism.[47,48] From table 1, it is confirmed that increasing concentration of K^+ ions into the $CaMoO_4$ host simultaneously increased the Yb^{3+} concentration (Tm^{3+} ions concentrations was too low to detect with precision). Second, the larger K^+ ions (r_{K^+}=0.152 Å and $r_{Ca^{2+}}$=0.114 Å) insertion into the $CaMoO_4$ matrix distort the crystal field around the Tm^{3+} ions, which can cause severe crystal field break or distortion around Tm^{3+} ions. This increases the 4f-4f transition probalities of Tm^{3+} ions and significantly increases the UC emission intensities.[42,49] The crystal field distortion is expected to be higher for K^+ ions compared to Li^+ and Na^+, and hence UC intensities increment is higher for the K^+ substitution eventhough all the metal ions showed significant incriment. From the supporting Fig. S1(b), it is clear that the deviation of lattice parameters a and V are significant while Ca^{2+} was substituted by K^+ ions compared to the other alkali metal ions. Further, it is assumed that under identical conditions, the degree of crystal distortion is reflected in the XRD peak broadening. We have carefully measured the XRD profile of 5 mol% M^+ ions (M= Li, Na, K, Rb) substituted $CaMoO_4$:0.1 mol% Tm, 10 mol% Yb samples and the full width half maximum (FWHM) values were calculated. The FWHM value, for example, for the 112 peak was found to be 0.13, 0.14, 0.18 and 0.22 for Li, Na, K and Rb, respectively. It further supports that the degree of crystal distortion order was Rb>K>Na>Li. The Rb^+ ions is extremely large, very difficult to occupy the Ca^{2+} ions site in the $CaMoO_4$ host (limit of solubility was less than 5 mol%) and hence the effect was not pronounced in the upconversion phenomenon. Particles morphology and packing densities is the another factor which governs the UC emission intensity. As shown in Fig. S5, the ball like phosphor samples exhibited higher UC intensities which is in the order of balls like particles > flakes like particles > rice grains like particles. Obviously, as the packing density decreases, the volume content of the phosphor decreases leading to decrease the UC emission intensity of the phosphor. The rice grains exhibited monodisperse particles with spongy texure and exhibited lowest densities. Further, the SEM micrographs in Fig. 2 supports that the packing densities is in the order balls > flakes > rice grains that determines the UC emission intensities.

Table 1
Elemental composition of $CaMoO_4$:0.1at% Tm^{3+}, 10at% Yb^{3+}, x at% K^+ measured by X-ray fluorescence spectroscopy (each sample was measured three times at different positions and data were averaged)

Sample	*Elemental composition (weight %)*				
	K_2O	*CaO*	*MoO_3*	*Yb_2O_3*	*Tm_2O_3*
CMO-0K	0.00	22.46	68.78	7.59	0.02
CMO-1K	0.07	22.29	68.87	8.01	0.03
CMO-5K	0.58	21.79	68.68	8.77	0.05
CMO-7K	0.98	21.19	68.61	8.97	0.06
CMO-10K	1.84	20.25	68.52	9.57	0.09

RSC Advances ARTICLE
www.rsc.org/advances

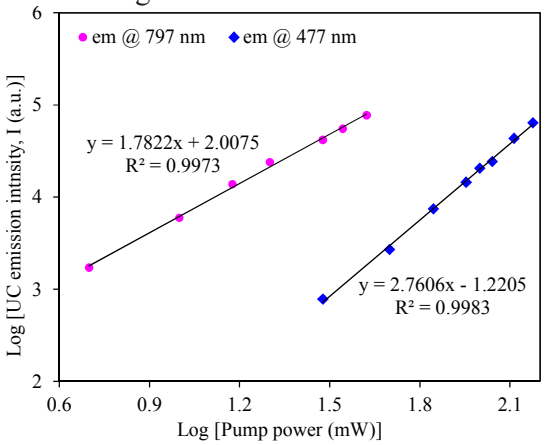

Fig. 6. Pump power dependence of UC emission (the NIR at 800 nm and blue at 477 nm) of $CaMoO_4$:0.1 mol% Tm^{3+}, 10 mol% Yb^{3+}, 10 mol% K^+ phosphors.

Fig. 6 shows the excitation power dependence of the blue and NIR emission of $CaMoO_4$:0.1 mol% Tm^{3+}, 10 mol% Yb^{3+}, 10 mol% K^+ phosphor recorded at room temperature. It is well known that for unsaturated UC processes, the number of photons required to populate the upper states can be obtained by the following general equation:[8,11,50]

$$I \alpha P^n$$

where n is a number of pumping photons required to excite the emitting state, I is the UC intensity and P is the laser pumping power. The calculated result (Fig. 6) indicates that the slope is ~1.78 for NIR and 2.76 for blue emissions. The n value for NIR (800 nm) emission ($^3H_4 \rightarrow {}^3H_6$ electronic trasition) is near to 2 and that of blue emission ($^1G_4 \rightarrow {}^3H_6$ electronic trasition) is near to 3. This result indicates that the NIR upconversion process involves two photons process whereas blue UC involves three photons.[34,42]

According to above results the upconversion mechanism of $CaMoO_4$:Tm^{3+},Yb^{3+},K^+ phosphor can be described as in Fig. 7. Under 980 nm lasers pumping, the $^2F_{5/2}$ of Yb^{3+} gets populated ($^2F_{7/2} \rightarrow {}^2F_{5/2}$). Then non-resonant energy transfer from the $^2F_{5/2}$ (of Yb^{3+}) level to the $^3H_5$ level of Tm^{3+} occurs. Alternatively, ground state absorption (GSA) process ($^3H_6 \rightarrow {}^3H_5$) can also populates $^3H_5$ level of Tm^{3+}. Subsequent $^3H_5 \rightarrow {}^3F_4$ transition can be induced by non-radiative multiphonon relaxation (designed by red dotted lines). Through the excited state absorption (ESA) or energy transfer upconversion (ETU) the $^3F_3$ state gets populated ($^3F_4 \rightarrow {}^3F_3$).[42,50,51] The $^3F_3$ state generates metastable $^3H_4$ state via non-radiative transition. The $^3H_4 \rightarrow {}^3H_6$ radiative transition gives rise to the NIR emission around 797 nm. The $^3H_4$ state can be further excited to the $^1G_4$ state through the ESA or ETU processes and the $^1G_4 \rightarrow {}^3H_6$ radiative transition gives rise to blue emission around 477 nm. Moreover, the $^3H_4$ states can be excited due to cross relaxation of $^1G_4 + {}^3F_4 \rightarrow {}^3H_4 + {}^3F_3$ transition, which populates the $^3H_4$ states and intensifies the NIR emission.[43] Furthermore, the energy gap of $^1G_4 \rightarrow {}^3H_4$ is smaller than the $^3F_4 \rightarrow {}^3F_2$. Therefore, $^1G_4 \rightarrow {}^3H_4$ can easily populate the $^3F_3$ state and the energy gap $^3F_3 \rightarrow {}^3H_4$ is so small , the $^3F_3$ state can easily populate the $^3H_4$ state by multi-phonon relaxation, as a consequence, the $^3H_4$ state gets over populated compared to $^1G_4$ state and hence the NIR emission intensity is much pronounced. Here, K^+ (or other alkali ions) distorts the crystal structaure in such a way that the energy states of Tm^{3+} ions arranges in such a way that the $^3H_4$ state get over populated than $^1G_4$ which is reflected as 47 fold intensification of NIR emission compared to the 7.8 fold in the blue band (Supporting Fig. S6).

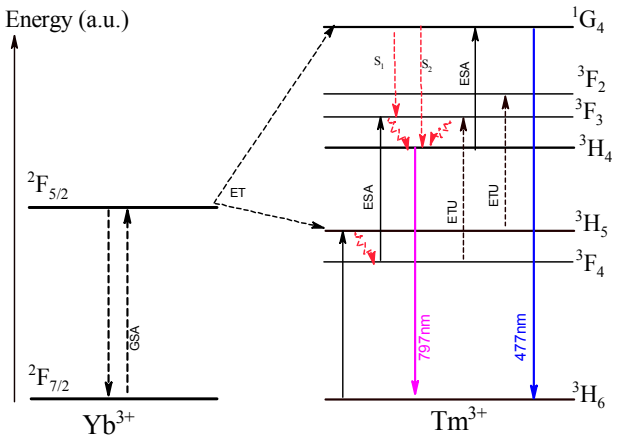

Fig. 7. Schematic energy diagram of $CaMoO_4$:Tm^{3+},Yb^{3+},K^+ phosphor and possible UC mechanism under 980 nm laser pump.

Thus, the K^+ substituted $CaMoO_4$:Tm^{3+},Yb^{3+} phosphor exhibits extremely intense UC at NIR (~797 nm) pumped by as low as 1 mW 980 nm laser power and can have potential application in the NIR bio imaging like photodynamic diagnosis where low power (<1mW) laser is recommended to reduce the laser induced harms.

4. Conclusion

A facile hydrothermal procedure has been developed to synthesize shape and size controlled $CaMoO_4$:Tm^{3+},Yb^{3+} upconversion phosphor. SEM images manifest that the phosphor consists of rice grains shape within nm dimensions. The NIR (797 nm) UC emission of Tm^{3+}/Yb^{3+} doped $CaMoO_4$ phosphor has been improved significantly by alkali ions doping and the order of increment is as; $K^+ > Na^+ > Li^+ >$ No alkali ion. The optimum concentrations of Tm^{3+}, Yb^{3+} and K^+ for the highest UC luminescence were 0.1 mol%, 10 mol% and 10 mol%, respectively. The UC emission mechanism was elucidated and found that two photon processes dominated the NIR emission while 3 photon processes governed the blue emission. The K^+ ions substitutions in the $CaMoO_4$ host led to distort the crystal field around Tm^{3+}, which significantly enhanced the UC emission intensity by more than 47 times. The brightest, $CaMoO_4$:0.1 mol% Tm^{3+}, 10 mol% Yb^{3+}, 10 mol% K^+ phosphor can be pumped by as low as 1 mW (980 nm) laser and can have potential applications not only bioimaging but also in displays, solar cell and catalysis.

Notes and references

[1]*Department of Advanced Technology Fusion, Saga University, Honjo-1, Saga, 850-8502, Japan.*
[2]*Shinwa-Biso Co., Ltd., 1-15-22, Moriguchi, Osaka, 570-003, Japan*
[#]*watarit@cc.saga-u.ac.jp (Takanori Watari)*
[*]*mehomnath@yahoo.com (Hom Nath Luitel)*
Tel.: +81 952 28 8683
Fax: +81 952 28 8548

1. J. Wang and P. Tanner, *J. Am. Chem. Soc.*, 2010, **132**, 947.
2. H.N. Luitel, R. Chand, K. Ikeue, T. Torikai, M. Yada and T. Watari, *Opt. Mater.*, 2014, **36,** 591.
3. F. Auzel, *C. R. Acad. Sci.*, 1966, **262**, 1016.
4. C. Strumpel, M. Mccann, G. Beaucarne, V. Arkhipov, A. Slaoui, V. Svrcek, C. del Canizo and I. Tobias, *Sol. Energy Mater. Sol. Cells*, 2007, **91**, 238.
5. M. Bass, A. Rapaport and H. Jennsen, *US Pat.*, 2003, 6654161.
6. E. Downing, L. Hesselink, J. Ralston and R. Macfarlane, *Science*,

1996, **273**, 1185.
7. F. Suyver and A. Meijerink, *Chemisch2Weekblad*, 2002, **98**, 12.
8. G.S. Yi and G.M. Chow, *Chem. Mater.,* 2007, **19**, 341.
9. H. Lin, G. Meredith, S.B. Jiang, X. Peng, T. Luo, N. Peyghambarian, and Y.B. Pun, *J. Appl. Phys.*, 2003, **93**, 186.
10. L.E. Enrico Cavalli, Jan Hostasa and M. Pedroni, *J. Eur. Ceram. Soc.*, 2013, **33**, 1425.
11. S. Heer, O. Lehmann, M. Haase and H.U. Goudel, *Angew. Chem., Int. Ed. Engl.*, 2003, **42**, 3179.
12. M. Seydack, *Biosens. Bioelectron.*, 2005, **20**, 2454.
13. A. Yuan , J. Wu, X. Tang, L. Zhao, F. Xu and Y. Hu, *J. Pharm Sci.,* 2013, **102**, 6.
14. X. Liu, Z. Ye, W. Wei, Y. Du, J. Yuan and D. Ma, *Chem Commun.*, 2011, **28**, 47.
15. R. Weissleder, *Nat. Biotechnol.*, 2001, **19**, 316.
16. R. Wang and F. Zhang, *J. Mater. Chem. B*, 2014, **2**, 2422.
17. E. D. Sternberg and David Dolphin, *Tetrahedron*, 1998, **54**, 4202.
18. M.V. DaCosta, S.Doughan, Y. Han and U.J. Krull, *Anal Chim. Acta.,* 2014, **832**, 1.
19. S. Wu, G. Han, D. J. Milliron, S. Aloni, V. Altoe, D. V. Talapin,B. E. Cohen and P. J. Schuck, *Proc. Natl. Acad. Sci. U.S.A.*, 2009, **106**, 10917.
20. M. Pokhrel, A.K. Gangadharan and D.K. Sardar, *Materials Letters,* 2013, **99**, 86.
21. I. Etchart, A. Huignard, M. Berard, M.N. Nordin, I. Hernandez, R.J. Curry, W.P. Gillin and A.K. Cheetham, *J. Mater. Chem.*, 2013, **20**, 3989.
22. G. Chen, T.Y. Ohulchanskyy, R. Kumar, H. Agren and P.N. Prasad, *ACS Nano*, 2010, **4**, 3163.
23. C. Li and J. Lin, *J. Mater. Chem.*, 2010, **20**, 6831.
24. M.C. Tan, L. Al-Baroudi and R.E. Riman, *Appl. Mater. Interfaces*, 2011, **3**, 3910.
25. F. Vetrone, R. Naccache, V. Mahalingam, C.G. Morgan and J.A. Capobianco, *Adv. Funct. Mater.*, 2009, **19**, 2924.
26. Q. Huang, J. Yu, E. Ma and K. Lin, *J. Phys. Chem. C,* 2010, 114, 4719.
27. D. Gao, X. Zhang, H. Zheng, P. Shi, L. Li and Y. Ling, *Dalton Trans.,* 2013, **42**,1834.
28. Q. Cheng, J. Sui and W. Cai, *Nanoscale*, 2012, **4**, 779.
29. Q. Huang, J. Yu, E. Ma and K. Lin, *J. Phys. Chem. C*, 2010, **114**, 4719.
30. X. Teng, Y. Zhu, W. Wei, S. Wang, J. Huang, R. Naccache and L. Huang, *J. Am. Chem. Soc.*, 2012, **134**, 8340.
31. Q. Dou and Y. Zhang, *Langmuir*, 2011, **27**, 13236.
32. A. K. Singh, S. K. Singh and S. B. Rai, *RSC advances*, 2014, **4**, 27039.
33. X. Li, F. Zhang and D. Zhao, *Chem. Soc. Reviews*, 2014, DOI: 10.1039/C4CS00163J
34. I. Etchart, I. Hernández, A. Huignard, M. Bérard, W.P. Gillin, R.J. Curry and A.K. Cheetham, *J. Mater. Chem.*, 2011, **21**, 1387.
35. A.M. Smith, M.C. Mancini, and S. Nie, *Nat. Nanotechnol.*, 2009, **4**, 710.
36. J.H. Chung, S.Y. Lee, K.B. Shim, S.Y. Kweon, S.C. Ur and J.H. Ryu, *Appl. Phys. A,* 2012, **108**, 369.
37. K. Mishra, N.K. Girl and S.B. Rai, *Applied Physics B - Laser and Optics*, 2011, **103**, 863.
38. V.C. Farmer, M. Society, *The infrared spectra of minerals, Mineralogical Society, London,* 1974.
39. F. Lei and B. Yan, *J. Solid State Chemistry*, 2008, **181**, 855.
40. S.P. Porto and J.F. Scott, *Phys. Rev.*, 1967, **157**, 716.
41. G. Madhusudana, P. Kumar, D.P. Kumar, V.S. Srikanth, M.V. Shankar, *Materials Letters*, 2014, **128**, 183.
42. W. Shi, S. Song and H. Zhang, *Chem. Soc. Rev.*, 2013, **42**, 5714.
43. A.M. Kaczmarek and R.V. Deun, *Chem. Soc. Rev.*, 2013, **42**, 8835.
44. J. Liu, H. Lian, and C. Shi, *Optical Materials*, 2007, **29**, 1591.
45. L.H.C. Andrade, M.S. Li, Y. Guyot, A. Brenier and G. Boulon, *Journal of Physics:Condensed Matter*, 2006, **18**, 7883.
46. A. Phuruangrat, T. Thongtem, S. Thongtem, *Journal of Alloys and Compounds*, 2009, **48**, 568.
47. S. Das, A.A. Reddy, G. V. Prakash, *Ceramics International*, 2012, **38**, 5769.
48. H.N. Luitel, T. Watari, R. Chand, T. Torikai and M. Yada, *J. Materials*, 2013, Article ID 613090.
49. B.R. Judd, *Phys. Rev.*, 1962, **127**, 750.
50. M. Pollnau, D.R. Gamelin, S.R. Luthi and H.U. Gudel, *Phys. Rev. B*, 2000, **61**,3337
51. J.J. Li, L.W. Yang, Y.Y. Zhang, J.X. Zhong, C.Q. Sun, P.K. Chu, *Opt. Mater.*, 2011, **33**, 882.

Graphical Abstract

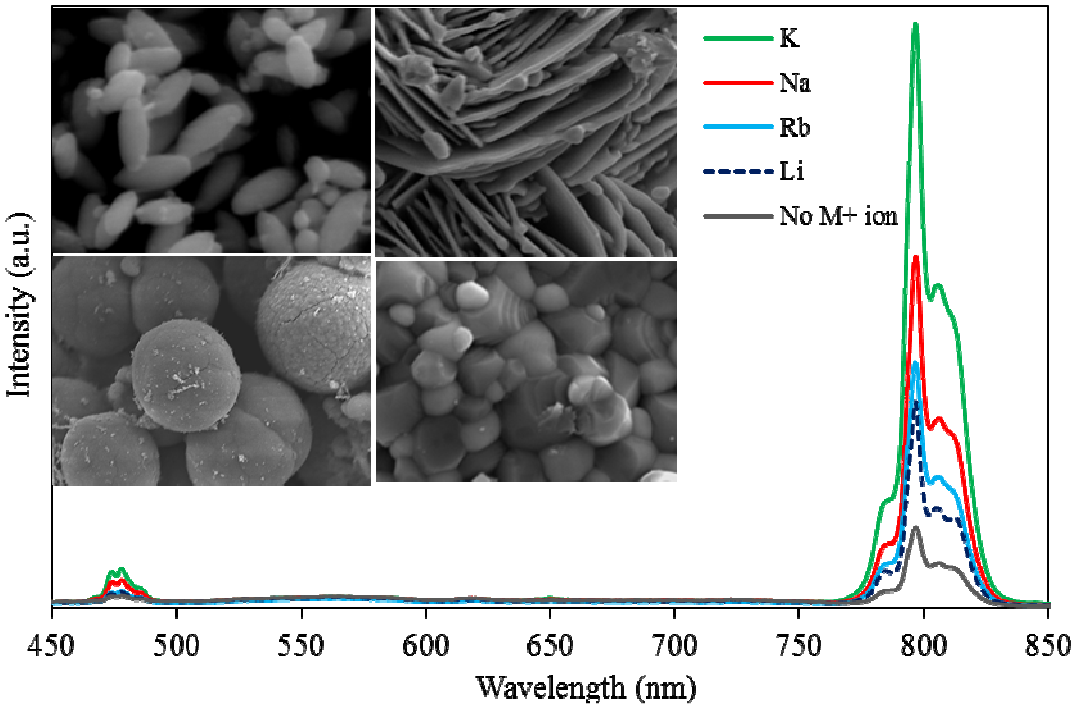

Highly efficient NIR to NIR upconversion in $CaMoO_4:Tm^{3+},Yb^{3+}$ nanocrystals pumped by less than 1mW laser was fabricated for biomedical applications.